



## OPEN

## SUBJECT AREAS:

SELF-ASSEMBLY

MOLECULAR SELF-ASSEMBLY

Received

4 August 2014

Accepted

16 December 2014

Published

15 January 2015

Correspondence and requests for materials should be addressed to Q.C. (qibinchen@ecust.edu.cn) or H.L. (hlliu@ecust.edu.cn)

# Hierarchical Assembly of a Dual-responsive Macroscopic Insulated Molecular Wire Bundle in a Gradient System

Yujie Sheng, Qibin Chen, Junyao Yao, Ying Wang &amp; Honglai Liu

Key Laboratory for Advanced Materials and Department of Chemistry, East China University of Science and Technology, Shanghai 200237, China.

Here, we report the hierarchical self-assembly of a cationic gemini amphiphile, Azo 1, in a composition gradient solution generated using solvent evaporation. As the gradient solution is formed, Azo 1 forms nanorods in the lower region of the solution. Depending on solvent composition, these nanorods can further develop into nanofibres, which can then intertwine to form double helices and other types of nanohelices in the upper region of the solution. Finally, a macroscopic wire bundle is formed via the fusion of nanohelices; this ribbon-like bundle exhibits elasticity and linear ohmic resistance properties. More intriguingly, this bundle exhibits photoresponsive properties that affect its deformation and conductivity, as well as a rapid electroresponse that affects its conductivity, indicating that it is feasible to control the charge pathway.

The spectacular rise of nanoscience has led to a remarkable trend of miniaturisation within the semiconductor industry<sup>1</sup>. The use of molecular devices, which provides an attractive alternative to the “top-down” method, signifies the potential of molecular-sized materials for electronic and photonic applications and has led to the development and probing of molecular-scale wires during the last two decades<sup>2–6</sup>. Insulated molecular wires (IMWS), which are capable of connecting two entities attached to their chain ends<sup>2,7</sup>, are expected to be applicable to bridging the gap between molecular-based electronic devices and macroscopic electrodes or to wiring a single molecule into an electrical circuit<sup>1,8–10</sup>. To date, various methods of IMWS fabrication have been explored<sup>7,11–15</sup>. One promising method is the one-dimensional (1D) self-assembly of  $\pi$ -conjugated molecular building blocks<sup>13–14</sup>. However, most  $\pi$ -conjugated assemblies of small organic molecules generate 1D objects within the nano- or micrometre scale<sup>16–17</sup>; thus, the synthesis of a long-range bridge between molecules and bulky electrodes remains challenging. Herein, we report a convenient synthetic route to the hierarchical self-assembly of a gemini amphiphile with an azobenzene core, (N,N'-((diazene-1,2-diyl bis (4,1-phenylene)) bis(methylene)) bis(N,N-dimethyl dodecan-1-aminium) bromide), here referred to as Azo 1 (Figure 1), into a macroscopic insulated wire bundle through the use of an evaporation-induced concentration gradient solution. The elasticity, conductivity and photoresponsive characteristics of this material are reported.

## Results and Discussion

Figure 1 summarises the hierarchical self-assembly of Azo 1. Due to the strong  $\pi$ - $\pi$  stacking of azobenzenes in a 2 : 1 dichloromethane/*n*-hexane mixture (*v/v*), Azo 1 self-assembles into oligomers in an organised manner by cofacial spiral stacking at a concentration of 0.31 mM. These oligomers can further extend, forming a nanorod and then a nanofibre with a helically wound columnar  $\pi$ -stack; this stack represents a primary assembling block, termed Agg<sub>1</sub>. During solvent evaporation, Agg<sub>1</sub>s tend to twist together to form a double-stranded secondary structure, termed Agg<sub>2</sub>. Next, several dozen Agg<sub>2</sub>s can further intertwine into a tertiary nanohelix structure with a diameter of approximately 50 nm, termed Agg<sub>3</sub>. Then, Agg<sub>3</sub>s, rather than intertwining, can fuse with each other into a ribbon-like quaternary structure with a width of approximately 200 to 600 nm, termed Agg<sub>4</sub>. Last, quinary macroscopic wire bundle structures with millimetre or even centimetre lengths are obtained by further fusion among Agg<sub>4</sub>s. This assembly is mainly directed by a combination of the “coil-rod-coil” molecular structure of Azo 1 and solvent evaporation, as confirmed by <sup>1</sup>H nuclear magnetic resonance (NMR), circular dichroism (CD) and ultraviolet-visible (UV-Vis) spectroscopy.

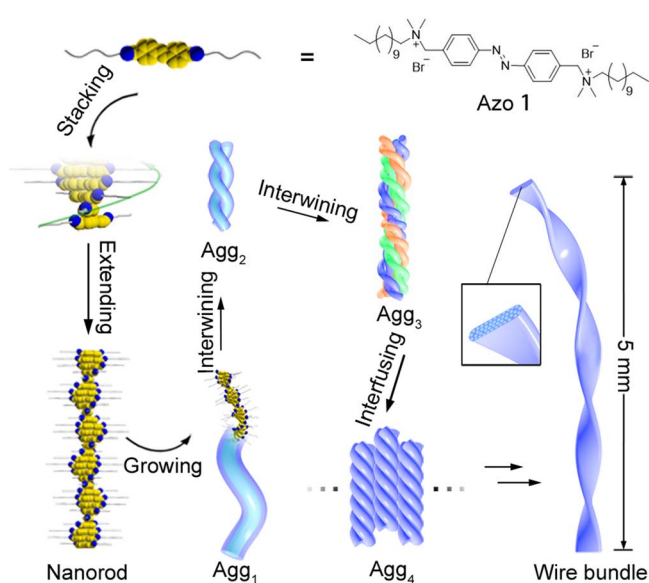


**Figure 1** | Schematic representation of the hierarchical self-assembly of Azo 1. The sub-structures of Agg<sub>3</sub> are coloured differently for clarity.

Azo 1 was synthesised with a *trans* configuration at the azobenzene moieties as detailed in the Supporting Information and was characterised using <sup>1</sup>H NMR and ESI mass spectrometry. Azo 1 self-assembled during solvent evaporation. After a 2-day evaporation period, the upper region of the solution darkened considerably, creating a vertical colour gradient (Figure 2a). However, when the solution was instead completely sealed with a ground glass joint for 2 days, no colour gradient was observed. Thus, Azo 1 becomes concentrated in the upper region during evaporation. Density measurements and refractive index results demonstrated that the upper and middle regions differed markedly and the lower and middle regions differed negligibly in solvent composition; this effect was ascribed to solvent evaporation. For refractive index analysis, HPLC grade solutions were used to obtain a working curve. The composition variation with the normalized height of the final solvent in a tube is recorded in Supplementary Fig. 1. Moreover, density measurements of the pure

and mixed solvents are similar under the same conditions, as shown in Figure 2a. Therefore, the upper, middle and lower regions were sampled separately, and transmission electron microscopy (TEM) and ultrahigh resolution field emission scanning electron microscopy (UHRFE-SEM) were used to visualise the structural transitions that occurred during assembly (Figure 2b to i).

Two structures, i.e., dots and nanorods, were found in the lower region; the dots formed as soon as Azo 1 was dissolved in the mixed solvent (Supplementary Fig. 2). The nearly linear array formed by the dots (Figure 2b, Inset) aided in their further assembly into nanorods with a uniform width of approximately 5 nm and a length of less than 100 nm (Figure 2b). Coincidentally, the width of these nanorods is consistent with the length of a fully extended molecule (4.4 Å). This observation, combined with the detection of a highly ordered zigzag alkyl chain conformation using attenuated total reflection-infrared (ATR-IR) spectroscopy (Supplementary Fig. 3), indicates that the Azo 1 molecules assembled linearly. Moreover, the rotational offset and cofacial distance between two neighbouring molecules were investigated by theoretical calculation and X-ray diffraction, according to previously reported methods<sup>18–19</sup>. The results show a 33° rotation offset and a stacking distance of 3.24 Å (Supplementary Fig. 4), indicating the nature of the helical supermolecules. In addition, in solutions that were sealed for 2 days, only the dot structure was observed (Supplementary Fig. 5). Therefore, nanorod formation was ascribed to solvent evaporation.

In contrast to the lower region, the upper region exhibited a variety of advanced aggregates. Primary nanofibres (Agg<sub>1</sub>) with lengths from 200 to 600 nm were observed (Figure 2c). Intriguingly, the widths of these nanofibres were consistent with those of the nanorods in the lower region, indicating that Agg<sub>1</sub> is derived from extension of the nanorods. After concentrating in the upper region, the nanorods associated along the longitudinal direction to form longer forms of Agg<sub>1</sub>. Moreover, these Agg<sub>1</sub>s intertwined to form a 10 nm-wide double-stranded secondary structure (Agg<sub>2</sub>) (Figure 2d, the white arrows indicate two Agg<sub>1</sub>s). Most importantly, a similar effect, in which two smaller nanofibrils intertwine to form a larger double helix, is shown in Figure 3 a to d; the diameters of these helices increased from 10 to 50 nm. This successive, multi-level assembly resulted in a tertiary nano-helix structure, Agg<sub>3</sub>, which exhibited a width of approximately 50 nm (Figure 2e, Figure 3d). The typical

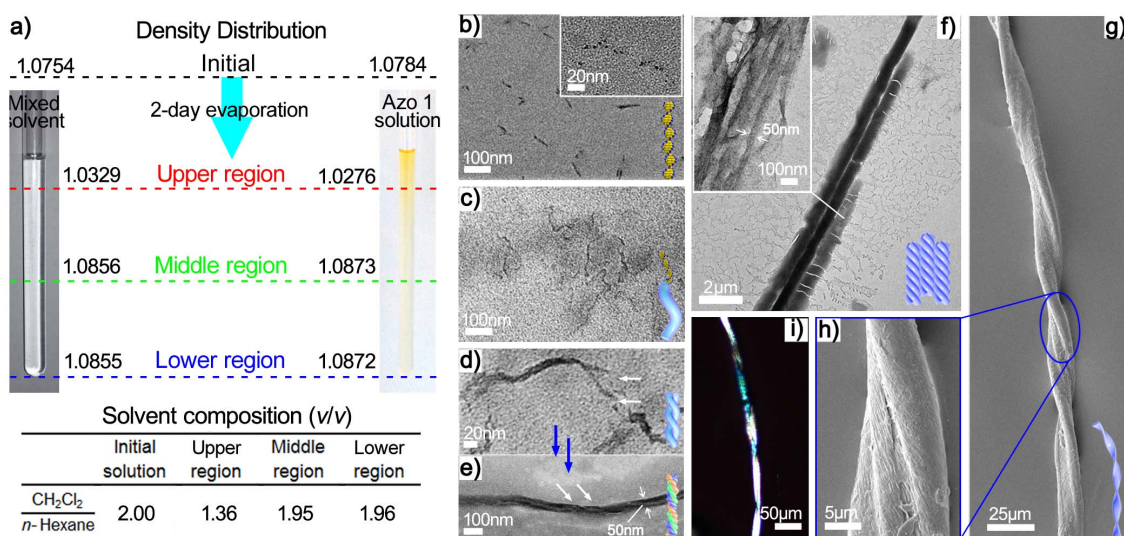


**Figure 2** | Morphologies of various aggregates that assembled in the gradient solution. (a) The density distribution of the gradient solution and the corresponding composition of each region. (b, c, d, e, f) TEM images of the aggregates in various stages from oligomers to nanoribbons (b, c, d and e after a 2-day evaporation and (f), after approximately 5 days of evaporation). (g) UHRFE-SEM images of the final bundle after approximately 7 days of evaporation. (h) Local amplification of the bundle shown in Figure 3f. (i) An image of the wire bundle obtained using polarised optical microscopy (POM).

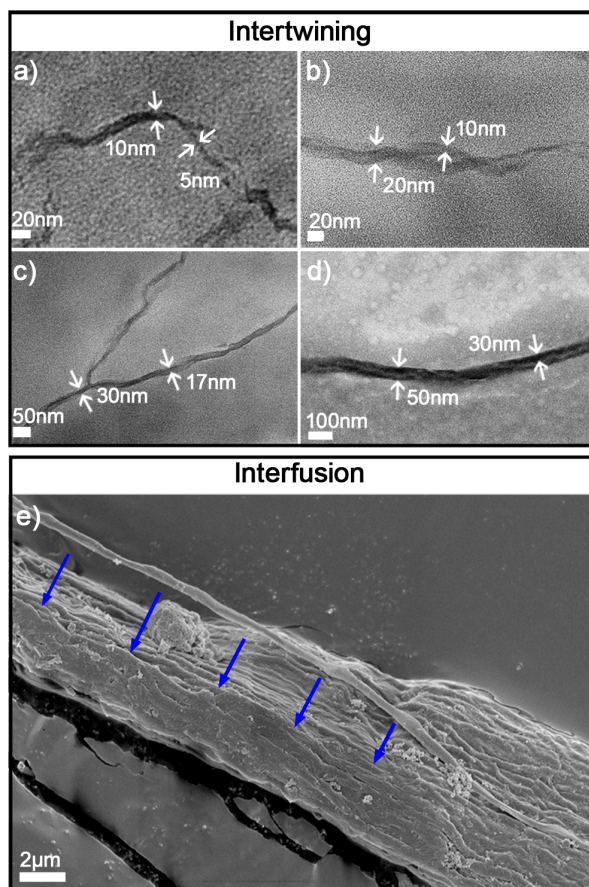


**Figure 3** | Intertwining of  $\text{Agg}_2$  and  $\text{Agg}_3$  (a, b, c and d) and interfusion of a ribbon-like structure,  $\text{Agg}_4$  (e). The blue arrows indicate a sub-aggregate that is joining the main aggregate.

helical structure of this structure is indicated by two arrows in Figure 2e.

In the middle region, however, we observed a ribbon-like quaternary structure,  $\text{Agg}_4$ ; this type of structure extended up to tens of micrometres in length with widths from 200 to 600 nm (Figure 2f) and comprised many parallel nanofibrils with widths of approximately 50 nm (Figure 2f, Inset). Therefore,  $\text{Agg}_4$  is attributed to the fusion of  $\text{Agg}_3$ s. If this assembly process continues,  $\text{Agg}_4$ s can form a macroscopic aggregate, as shown in Figure 2f. The fusion of  $\text{Agg}_4$  was confirmed using UHRFE-SEM (Figure 3e). Finally, as expected, macroscopic wire bundles sedimented or became attached to the test tube wall. Such bundles were found in a coiled configuration with two opposite-handed helices connected by a helical twist (Figure 2g). The local amplification (Figure 2h) exhibited by the twist bundle comprised three sub-bundles, which consisted of a close, parallel array of smaller wires with diameters of several hundred nanometres. Additionally, the bundle was highly crystalline, as shown by POM observations, suggesting that it forms an ordered structure (Figure 2i).

The structural transition of Azo 1 aggregates can be observed using spectroscopy. NMR showed that Azo 1 is prone to aggregation in weakly polar solvents (e.g.,  $\text{CDCl}_3$ ) (Figure 4a). Three pairs of doublets (red, yellow and green dots) at 7.6–8.0 ppm indicate the coexistence of three types of aromatic protons in different environments, i.e., the individual (red box), cap (green boxes) and inner (yellow box) molecules in an oligomer. This phenomenon can be ascribed to the shielding effect of  $\pi$  electrons in adjacent molecules<sup>20–21</sup>. Due to the enhancement of shielding that results from the intensity of  $\pi$ - $\pi$  stacking, peak pairs are gradually upshifted ( $\delta$  becomes smaller).

Additionally, the shifted peaks assigned to methylene groups at 5.5–5.7 ppm can be attributed to corresponding environments based on  $^1\text{H}/^1\text{H}$  nuclear Overhauser effect spectra (Supplementary Fig. 6). A higher concentration (2.5 mM) was used to obtain optimal resolution in the NMR experiments. A similar phenomenon can be observed in a dilute solution (0.31 mM, identical to that used in the assembly), although two doublets with smaller values of  $\delta$  were overlapped (Supplementary Fig. 7). The observed coexistence of monomers and oligomers based on the  $^1\text{H}$  NMR spectrum indicates that pre-aggregates can be formed when Azo 1 is dissolved in chloroform or in a  $\text{CH}_2\text{Cl}_2/n$ -hexane mixture, which is consistent with the TEM observations.

After a 2-day period of evaporation, the upper, middle and lower regions of the tube were sampled separately. UV-Vis spectra (Figure 4b) showed that the concentration of Azo 1 was increased slightly in the lower and middle regions after solvent evaporation but increased markedly in the upper region, indicating enrichment in the upper region or the formation of a non-uniform solution in the tube. This result is also confirmed by GC-MS experiment (Supplementary Fig. 8). Positive CD bands (Figure 4b) suggest that the azobenzene groups in the aggregates experienced a helical environment; thus, we proposed a helically arranged model<sup>22–23</sup>. In addition, the variation of CD signals among the different solution regions after solvent evaporation demonstrates that the aggregates experienced a structural transition.

Together, these results demonstrate that Azo 1 undergoes a remarkable hierarchical self-assembly in the gradient solvent. Azo 1 demonstrated an extreme tendency to aggregate in weak polar solvents due to its unique “coil-rod-coil” molecular structure. In weak polar solvents, apolar alkyl chains (coil moieties) promptly adopted extended geometry due to their solvation; thus, Azo 1 appeared as a nearly linear conformation. However, the head groups would be exposed to the organic media in such a structure, which would be energetically unfavourable. As a compromise, a helically wound columnar  $\pi$ -stack, which attenuates the contact between the head groups and the organic environment, was formed by  $\pi$ - $\pi$  stacking and electrostatic attractions between the head groups and counter ions. Solvent evaporation generated a gradient due to the difference in evaporation capacity between  $\text{CH}_2\text{Cl}_2$  and  $n$ -hexane, as supported by the refractive index results and density measurements (Figure 2a). After a 2-day evaporation period, the volume ratios in the upper, middle and lower regions became approximately 1.36 : 1, 1.95 : 1 and 1.96 : 1, respectively; thus, the upper region exhibited the weakest polarity. Therefore, aggregates (dots and nanorods) tended to accumulate in a weak polar region, i.e., the upper region ( $v_{\text{DCM}}:v_{n\text{-Hexane}} = 1.36:1$ ), due to increased solvation of the alkyl chains, leading to a higher concentration of Azo 1. These aggregates can associate in two ways, longitudinally and laterally, to further minimise the contact between the head groups and the solvent. Longitudinal association leads to the formation of longer aggregates, such as  $\text{Agg}_1$ , whereas lateral association results in the formation of the wider aggregates ( $\text{Agg}_i, i = 2, 3, 4$  and 5). Regarding lateral assembly, the intertwining is driven by the overwinding of  $\text{Agg}_1$ ; thus, the longer alkyl chains and broader spacer groups provide  $\text{Agg}_1$  and  $\text{Agg}_2$  with increased ability to twist into helical shapes<sup>24</sup>. These two assembly ways coexist in the upper region (approximately accounting for 10% from the interface, as shown in Supplementary Fig 1). After successive multi-level intertwining,  $\text{Agg}_3$  may consist of tens of linearly  $\pi$ -stacked aromatic cores, forming stiff aggregates with low flexibility; thus, it is difficult for  $\text{Agg}_3$  to intertwine further. Nevertheless, the lateral fusing of  $\text{Agg}_3$ s provides a feasible alternative to such intertwining; thus subaggregates can gradually enlarge in the gradient region, leading to the formation of  $\text{Agg}_4$  approximately in the middle region with the DCM/ $n$ -hexane ratio of  $\sim 1.95:1$  ( $v:v$ ).  $\text{Agg}_4$  might be located in this region because it is too heavy to remain in the upper region as its size increases.

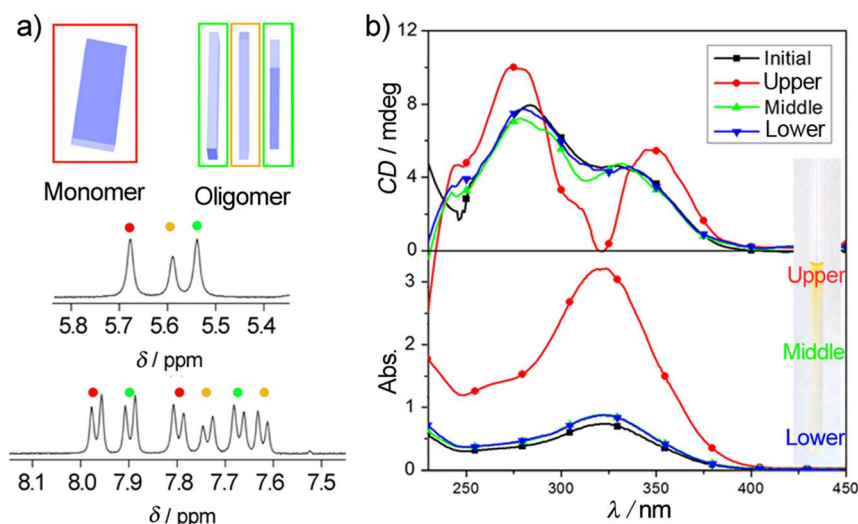


**Figure 4** | The assembly process and aggregate enrichment as measured based on NMR spectra. (a) Stacked  $^1\text{H}$  NMR spectra and corresponding schematic representations of 2.5 mM Azo 1 dissolved in  $\text{CDCl}_3$ . The blue block stands for the conjugated moiety of Azo 1. (b) CD and UV-Vis spectra of Azo 1 in the bulk solution before and after solvent evaporation for 2 days. (Here,  $C = 0.08$  mM. For the upper region, the sample was diluted with equal amounts of solvent because CD signals exceeded the measurable range, and the solution was maintained at  $25.0 \pm 0.2^\circ\text{C}$ .)

Finally, after further interfusion,  $\text{Agg}_4$  can generate a macroscopic wire bundle in the middle region or the lower region. In summary, Azo 1 first intertwists at the microscopic scale; then, it interfuses from the microscopic to the mesoscopic scale; and finally, it is visible at the macroscopic level. This process is remarkably different than processes based solely on intertwining<sup>23</sup> or fusion<sup>25</sup>. Based on this property, the formed wire bundles can potentially play a bridging role in micro-macro circuits.

The resultant ribbon is a bundle of nanohelices comprising rigid azobenzene cores surrounded by flexible insulated sheaths, which enables useful mechanical and electrical properties. As shown in Figure 5a, a wire bundle was fixed at one end while a stainless steel rod was used to pull the ribbon. After removal of the rod, the wire bundle immediately recovered its initial shape, demonstrating that the bundle is elastic. By considering the molecular structure, it can be deduced that the helically wound columnar  $\pi$ -stack of aromatic cores, intertwisting nanofibrils and the interfusing nanohelices and mesoribbons act synergistically to provide this elasticity.

Photo-responsive deformation was also investigated due to the presence of a photoswitchable azobenzene core (Figure 5b). It was observed that the wire bundle gently bends at its tip under irradiation at 302 nm and recovers its initial state under irradiation at 405 nm. The deformation and recovery require approximately 120 min and 160 min, respectively, and are remarkably faster than those measured for other bulky self-assembled aggregates, such as single crystals of an azobenzene derivative<sup>26</sup>. To the best of our knowledge, this is the first attempt to construct a promising shape memory material based on a small molecule rather than general polymers<sup>27</sup>.

Finally, the conductivity of the wire bundle was characterised. We first fabricated a device with a graphite electrode (Figure 5c) that had a leakage current of less than 20 nA at 10 V (Figure 5d, black line). Due to the strong stacking pathway surrounded by the insulated alkyl sheath, the ribbon can conduct electricity in the stacking direction. Therefore, a drop of saturated KCl was used as a junction to guarantee thorough contact and to reduce the contact resistance to a minimum. This two-terminal device, with channel and interface contacts in series, exhibited a linear ohmic resistive behaviour and higher conductivity values than an amorphous film, as shown using I/V measurements (blue line in Figure 5c and Supplementary Fig. 9). The total resistance of the device was approximately 6.7 M $\Omega$ , which is comparable to that of inorganic gallium nitride (approximately

10 M $\Omega$ ). However, the electrical conductivity of 3.98  $\text{S m}^{-1}$  is not as high as that achieved using one of the most successful  $\pi$ -conjugated wires by Faramarzi<sup>9</sup>. However, our bundle is nearly  $2 \times 10^5$  times longer than that obtained by Faramarzi et al. and defects are unavoidable during the assembly of such long and large wire bundles and are the main cause of impaired charge transportation. Intriguingly, the resistance of the devices can be reversibly influenced by exposure to alternating UV/Vis irradiation. After UV irradiation for over 2 hours, the conductivity was reduced to 2.12  $\text{S m}^{-1}$  (Figure 5, green line). This can be ascribed to a *trans* to *cis* transformation, which temporarily introduces disorder and interrupts the pathways for charge mobility. In contrast, 3 hours later, upon exposure to irradiation at 405 nm, the conductivity recovered to the original value of 3.98  $\text{S m}^{-1}$ . In addition, we unexpectedly observed that the conductivity was recovered after four continual linear sweeps within approximately 2 minutes, even when visible light is not used (Supplementary Fig. 10); this finding suggests the possibility of an electronically driven *cis* to *trans* isomerisation. These results imply that our bundle is able to act not only as a promising micro-macro bridge but also as a photo- or electro-responsive component.

## Conclusions

In conclusion, we utilised solvent evaporation of a mixed solvent as an effective and convenient method of achieving hierarchical self-assembly from the molecular to macroscopic scale. Solvent evaporation can induce a solvent concentration gradient, lead to a differences in solute content and the distribution of monomers; these differences cause a structural transformation from nanorods to a macroscopic wire bundle. The shape memory effect, photo- and electro-responsive behaviour and conductive property of the resulting bundle are attributed to the hierarchically assembly, the azobenzene core and its linear  $\pi$ -stacking. Our method provides a promising protocol for forming bridges between nano and macro devices.

## Methods

**Materials and General Measurement.** The preparation and characterisation of Azo 1, general measurement methods and computational details are summarised in the Supplementary Information.

**Apparent Elasticity Assessment.** To obtain an approximate measure of elasticity, the macroscopic bundle was placed on a glass slide and anchored at one end using silicone grease. A stainless steel rod was used to pull the bundle. The resulting shape deformation was recorded by a CCD camera, which was located over the slide.

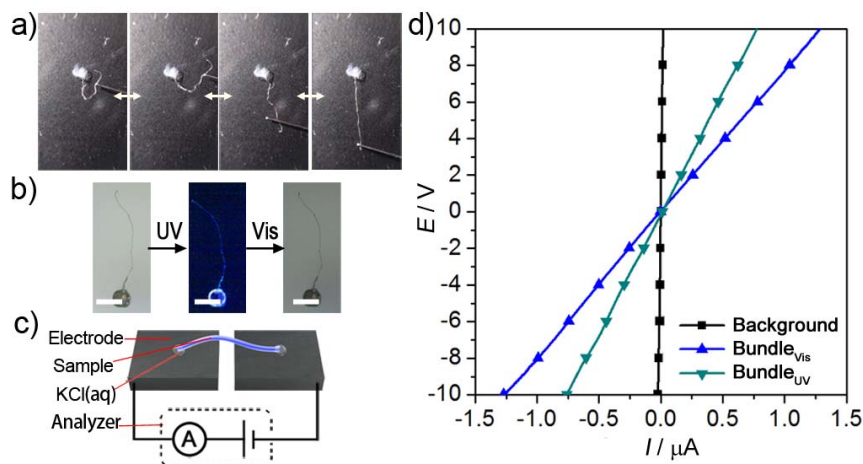


**Figure 5 | Elasticity and conductivity of the wire bundle.** (a) Elastic assessment of the wire bundle. (b) Photo-induced shape memory effect (Scale bar: 1 mm). (c) Conductive measurement and (d) the conductivity of the wire bundle. Animations of (a) and (b) are available as Supplementary Movies 1 and 2.

**Photoresponsive Deformation.** Photoresponsive deformation was performed using a 302 nm UV light (fluorescent lamp, 8 W) at a distance of 2 cm and using a 410 nm visible light (laser source, 120 mW, adjustable spot size) at a distance of 10 cm. The bundle was placed vertically, and the deformation was recorded by a horizontal CCD camera equipped with a 5X adjustable objective lens.

**Conductive Experiments.** The bundle conductivity was measured by placing each tip of the bundle onto a graphite electrode plate. Then, a drop of saturated potassium chloride solution was added to each electrode to guarantee full conductivity between the bundle and the electrode. Regarding the amorphous film, a 1% (w/w) dichloromethane solution was dropped onto indium tin oxide (ITO) glass until the solution covered the entire plate. After the solvent had evaporated, an amorphous film remained. A drop of saturated potassium chloride solution was added between the film and the columnar graphite electrode to ensure circuit conductivity. Linear sweep voltammetry was measured using a PARSTAT 4000 (Princeton Applied Research, USA).

**Self-assembly of the Bundle.** A 10-mg sample was dissolved in 40 ml of mixed solvent ( $\text{CH}_2\text{Cl}_2$ : *n*-hexane = 2:1). The solution was processed by ultrasonication for 20 min and then filtered through a 0.22- $\mu\text{m}$  PTFE syringe filter. The filtrate was injected into a glass tube, which was covered with polypropylene film and incubated at  $25.0 \pm 0.2^\circ\text{C}$ . After a several-day evaporation period, the macroscopic bundle was carefully chosen from the sample suspension with the aid of a stereoscopic microscope, and residual solute was removed.

- Joachim, C., Gimzewski, J. K. & Aviram, A. Electronics using hybrid-molecular and mono-molecular devices. *Nature* **408**, 541–548 (2000).
- Creager, S. *et al.* Electron Transfer at Electrodes through Conjugated “Molecular Wire” Bridges. *J. Am. Chem. Soc.* **121**, 1059–1064 (1999).
- Giacalone, F., Segura, J. L., Martín, N. & Guldi, D. M. Exceptionally small attenuation factors in molecular wires. *J. Am. Chem. Soc.* **126**, 5340–5341 (2004).
- Kim, F. S., Ren, G. & Jenekhe, S. A. One-Dimensional Nanostructures of  $\pi$ -Conjugated Molecular Systems: Assembly, Properties, and Applications from Photovoltaics, Sensors, and Nanophotonics to Nanoelectronics. *Chem. Mater.* **23**, 682–732 (2011).
- Villares, A. *et al.* The use of scanning polarization force microscopy to study the miscibility of a molecular wire candidate and an insulating fatty acid in mixed LB films. *Soft Matter* **4**, 1508–1508 (2008).
- Ortony, J. H. *et al.* Internal dynamics of a supramolecular nanofiber. *Nat Mater* **13**, 812–816 (2014).
- Terao, J. *et al.* Insulated molecular wire with highly conductive  $\pi$ -conjugated polymer core. *J. Am. Chem. Soc.* **131**, 18046–18047 (2009).
- Feldman, A. K., Steigerwald, M. L., Guo, X. & Nuckolls, C. Molecular electronic devices based on single-walled carbon nanotube electrodes. *Acc. Chem. Res.* **41**, 1731–1741 (2008).
- Faramarzi, V. *et al.* Light-triggered self-construction of supramolecular organic nanowires as metallic interconnects. *Nat. Chem.* **4**, 485–490 (2012).
- Sugiyasu, K. *et al.* A self-threading polythiophene: defect-free insulated molecular wires endowed with long effective conjugation length. *J. Am. Chem. Soc.* **132**, 14754–14756 (2010).
- Li, C. *et al.* Self-assembly of supramolecular chiral insulated molecular wire. *J. Am. Chem. Soc.* **127**, 4548–4549 (2005).

- Maniam, S. *et al.* Molecular fibers and wires in solid-state and solution self-assemblies of cyclodextrin [2] rotaxanes. *Org. Lett.* **10**, 1885–1888 (2008).
- de Hatten, X., Asil, D., Friend, R. H. & Nitschke, J. R. Aqueous self-assembly of an electroluminescent double-helical metallopolymer. *J. Am. Chem. Soc.* **134**, 19170–19178 (2012).
- Rosokha, S. V., Stern, C. L. & Ritzert, J. T.  $\pi$ -Bonded molecular wires: self-assembly of mixed-valence cation-radical stacks within the nanochannels formed by inert tetrakis [3, 5-bis (trifluoromethyl) phenyl]borate anions. *Cryst. Eng. Comm.* **15**, 10638–10638 (2013).
- Masai, H. *et al.* Synthesis of one-dimensional metal-containing insulated molecular wire with versatile properties directed toward molecular electronics materials. *J. Am. Chem. Soc.* **136**, 1742–1745 (2014).
- Yan, D., Zhou, Y. & Hou, J. Supramolecular self-assembly of macroscopic tubes. *Science* **303**, 65–67 (2004).
- Che, Y., Datar, A., Balakrishnan, K. & Zang, L. Ultralong nanobelts self-assembled from an asymmetric perylene tetracarboxylic diimide. *J. Am. Chem. Soc.* **129**, 7234–7235 (2007).
- Fink, R. F. *et al.* Exciton trapping in  $\pi$ -conjugated materials: a quantum-chemistry-based protocol applied to perylene bisimide dye aggregates. *J. Am. Chem. Soc.* **130**, 12858–12859 (2008).
- Néabo, J. R., Rondeau-Gagné, S., Vigier-Carrière, C. & Morin, J.-F. Soluble conjugated one-dimensional nanowires prepared by topochemical polymerization of a butadiynes-containing star-shaped molecule in the xerogel state. *Langmuir* **29**, 3446–3452 (2013).
- Nam, S. R., Lee, H. Y. & Hong, J.-I. Control of macroscopic helicity by using the sergeants-and-soldiers principle in organogels. *Chem-eur. J.* **14**, 6040–6043 (2008).
- Shi, M.-M. *et al.*  $\pi$ - $\pi$  Interaction among violanthrone molecules: observation, enhancement, and resulting charge transport properties. *J. Phys. Chem. B* **115**, 618–623 (2011).
- Huang, Z. *et al.* Pulsating tubules from noncovalent macrocycles. *Science* **337**, 1521–1526 (2012).
- Yagai, S. *et al.* Control over Hierarchy Levels in the Self-Assembly of Stackable Nanotoroids. *J. Am. Chem. Soc.* **134**, 18205–18208 (2012).
- Wu, G. *et al.* Bolaamphiphiles Bearing Bipyridine as Mesogenic Core: Rational Exploitation of Molecular Architectures for Controlled Self-Assembly. *Langmuir* **28**, 5023–5030 (2012).
- Zhang, X., Görl, D., Stepanenko, V. & Würthner, F. Hierarchical growth of fluorescent dye aggregates in water by fusion of segmented nanostructures. *Angew. Chem. Int. Edit.* **53**, 1270–1274 (2014).
- Bushuyev, O. S., Tomberg, A., Friščić, T. & Barrett, C. J. Shaping Crystals with Light: Crystal-to-Crystal Isomerization and Photomechanical Effect in Fluorinated Azobenzenes. *J. Am. Chem. Soc.* **135**, 12556–12559 (2013).
- Lee, B. K. M. *et al.* Tailoring the Photomechanical Response of Glassy, Azobenzene-Functionalized Polyimides by Physical Aging. *Macromolecules* **45**, 7527–7534 (2012).

## Acknowledgments

This work is supported by the National Natural Science Foundation of China (No.21273074, 91334203), the 111 Project of China (No.B08021) and the Fundamental Research Funds for the Central Universities of China (WK1213003). We appreciate Dr.



LieLie Li for his aid of compound synthesis, Dr. Jie Zhu and Dr. Pengwei Jin for  $1\text{H}/1\text{H}$  NOESY analysis and Prof. Shizhong Yang for GC-MS assessment.

### Author contributions

Y.S. and Q.C. conceived the project and wrote the paper, Y.Y. performed the PES computation, Y.W. and H.L. reviewed the manuscript. All authors read and approved the manuscript.

### Additional information

Supplementary information accompanies this paper at <http://www.nature.com/scientificreports>

**Competing financial interests:** The authors declare no competing financial interests.

**How to cite this article:** Sheng, Y., Chen, Q., Yao, J., Wang, Y. & Liu, H. Hierarchical Assembly of a Dual-responsive Macroscopic Insulated Molecular Wire Bundle in a Gradient System. *Sci. Rep.* 5, 7791; DOI:10.1038/srep07791 (2015).



This work is licensed under a Creative Commons Attribution-NonCommercial-NoDerivs 4.0 International License. The images or other third party material in this article are included in the article's Creative Commons license, unless indicated otherwise in the credit line; if the material is not included under the Creative Commons license, users will need to obtain permission from the license holder in order to reproduce the material. To view a copy of this license, visit <http://creativecommons.org/licenses/by-nc-nd/4.0/>